Article

Comparison of Noise Impact from Aircraft Flyover Measurements and Simulations Considering Model Uncertainties

Felix Lößle *, Lothar Bertsch [ID] and Rainer Schmid

German Aerospace Center (DLR), Institute of Aerodynamics and Flow Technology, 37073 Göttingen, Germany; lothar.bertsch@dlr.de (L.B.); rainer.schmid@dlr.de (R.S.)
* Correspondence: felix.loessle@dlr.de

Abstract: This paper presents a comparison of acoustic flyover measurements conducted using DLR's Advanced Technology Research Aircraft for different aircraft configurations with simulations performed in the Parametric Aircraft Noise Analysis Module. The focus of the comparison is on quantifying the simulation uncertainty arising from the source models used to describe the individual noise components (model uncertainty). Combining the comparison of measurements and simulations with the model uncertainty analysis allows for the identification of systematic deviations and modelling insufficiencies in the simulation. Based on eight different aircraft flyover configurations, the study demonstrates that the simulations match the measurements very well in six cases. The deviations observed in the remaining two cases can be attributed to the selected source model for the slat.

Keywords: aircraft noise simulation; uncertainty; PANAM; ATRA

1. Introduction

Noise simulations of departing and landing aircraft have been conducted for several years, among others by the German Aerospace Center (DLR) using the *Parametric Aircraft Noise Analysis Module* (PANAM) [1], by NASA using the *Aircraft Noise Prediction Program* (ANOPP) [2], by Empa using sonAIR [3,4], and by JAXA [5–7]. To compare simulation results with aircraft noise measurements and assess the quality of the simulation models, it is essential to quantify the underlying simulation uncertainty. The definition of uncertainty in noise simulations differs from that in noise measurements. Measurements exhibit both random and systematic errors. Random errors arise from variations in environmental conditions and measurement inaccuracies. They can be reduced through repeated measurements. Systematic errors, in contrast, act in the same direction in every repetition of the measurement and therefore cannot be eliminated by repetition. Systematic errors must be avoided by the experimenter through careful preparation and diligent execution of the experiments.

Simulations are not subject to random errors. However, simulation uncertainty arises firstly from uncertainties in the input parameters (e.g., aircraft mass, flight altitude, engine power setting), referred to as input uncertainty, and secondly from the fact that the source models used for simulating individual noise components do not represent the real noise emission perfectly due to model assumptions and simplifications, referred to as model uncertainty [8–10].

The comparison of noise simulations with measurements contributes to the evaluation of simulation quality [11–13]. However, such comparisons alone, without an analysis of uncertainties, do not provide information on the potential spread of simulation results or on the sensitivity of the outcome to variations in input parameters.

The consideration of uncertainties in aircraft noise simulation using the DLR tool PANAM began in 2019 [8]. In this study, the input and model uncertainties of the single-event noise models in PANAM were quantified using a first-order second-moment (FOSM) approach. Later, Römer et al. [9] compared the FOSM method for uncertainty estimation with Monte Carlo simulations and higher-order polynomial chaos methods, demonstrating that the FOSM approach provides reliable uncertainty estimates for PANAM at the lowest computational cost. In Bertsch et al. [10], the uncertainty of flight trajectories simulated with FLIPNA was included in the analysis for the first time, using the example of a supersonic business jet. Since this investigation employed two simulation tools, PANAM and FLIPNA, the problem could no longer be addressed using the FOSM approach, and a Monte Carlo simulation was therefore conducted.

Considering uncertainties is of particular importance for future aircraft concepts such as supersonic aircraft. As these designs are still in the preliminary development stage, the quality of the input data required for noise simulations is lower, i.e., higher input uncertainty. In addition, the source models for individual noise components are not tailored to the specific aerodynamics and propulsion technologies of such aircraft (e.g., delta wings, engines with low bypass ratio). This leads to larger model uncertainties compared to well-studied conventional aircraft. For supersonic aircraft, uncertainty studies have been conducted by DLR [10], NASA [14–17], and JAXA [5–7]. The comparison of the studies shows that, despite the novelty of the aircraft design, the computed uncertainties of the three research institutes are remarkably similar.

When conducting studies on airport noise reduction with current aircraft, a comprehensive understanding of the influence of model uncertainties is important. Therefore, the aim of the present study is to investigate model uncertainties isolated from other sources of uncertainty. This is achieved by comparing simulations with data obtained from flyover measurements under flight conditions that are accurately known and associated with only minimal uncertainties. Measurement data fulfilling these criteria were acquired during a campaign in Cochstedt using DLR's A320 research aircraft (Advanced Technology Research Aircraft, ATRA). Operational parameters such as flight altitude, speed, engine rotational speed, and configuration are well known with only little uncertainty [18–20]. However, the acoustic measurement chain is subject to uncertainties. Calibration measurements have shown that the uncertainty of free-field microphone measurements ranges between 0.36 dB and 0.52 dB [21]. A digital aircraft model of the ATRA including the engine performance map is available and enables a full-blown simulation, i.e., flight performance, operating conditions, and noise prediction [13]. Due to the low flyover altitude of approximately 200 m, the influence of the atmosphere on the transmission to the microphones is negligible. Consequently, aircraft noise simulations were conducted under standard atmospheric conditions. As a consequence of the high quality of the measurement data and the validated digital aircraft model, it can be assumed that deviations of the input data from the real aircraft and environment are very small, i.e., no input uncertainty is accounted for.

The campaign comprised flyover measurements at idle thrust. Jet noise was included in the simulations. However, the simulations showed that it does not contribute to the total sound pressure level SPL. Therefore, jet noise is not further discussed in the present study. Fan noise and aerodynamic noise sources are of the same order of magnitude, and their noise ranking depends on the operating condition. Therefore, these measurement data are

well suited to investigate the sensitivity of the various source models integrated in PANAM with respect to noise impact and to estimate the total uncertainty of the simulation results.

2. Aircraft

The flyover measurements were conducted using the Airbus A320-232 ATRA operated by DLR [18–20]. The ATRA, shown in Figure 1 as sketch of the digital model, serves as a flight test platform that can be flexibly adapted to various research missions. It is equipped with IAE V2500 engines, each providing a maximum thrust of 111 kN. Table 1 summarizes the major specifications of the aircraft. The ATRA features a data acquisition system that records position data, true airspeed (TAS), and engine rotational speeds.

The digital twin of the ATRA for noise prediction was generated using the aircraft design code *Preliminary Aircraft Design and Optimization* (PrADO), developed at TU Braunschweig [22–25]. The engine performance map of the IAE V2500 was obtained from the external tool GTlab, which is developed by the DLR Institute of Propulsion Technology [26]. A comparison of the digital twin to available aircraft data showed good agreement [25]. The mean deviation of the simulation of the maximum sound pressure level from the measurement for all studied flyovers was 0.64 dB. However, the differences depended on the flight configuration (flap, slat, and gear position). For some flight conditions, the mean differences reached up to 1.33 dB [13].
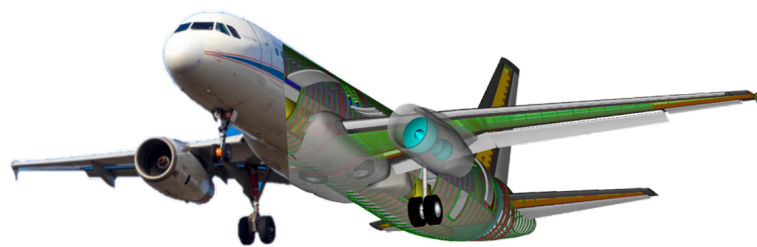

Figure 1. Sketch of the digital model of DLR's experimental aircraft ATRA.

Table 1. Major specifications of DLR's ATRA [27].

Airbus A320-232	
Length	37.57 m
Wingspan	34.10 m
Operating empty weight	43.3 t
Maximum takeoff mass	75.5 t
Engines	IAE V2500
Engine thrust	111 kN per engine

3. Flyover Measurements

The flyover measurements were conducted in 2016 at the Cochstedt test airfield [18–20]. A data acquisition system is installed on the ATRA that records position data, true airspeed, and engine rotational speeds. In addition to recording the aircraft's position with ATRA's onboard data acquisition system, the altitude was determined using a ground-based camera system. By calibrating the onboard position data with the measurements from the ground-based camera system, the accuracy of the position determination could be significantly improved. For this study, the associated input data uncertainty was neglected.

To measure the impact of ground noise, 27 ground microphones were placed along the runway beneath the flight path. As illustrated in Figure 2, the microphones were arranged in three rows under the flight path. The outermost microphones were positioned laterally at a distance of 170 m from the flight path. For this analysis, only the data recorded by

the centerline microphones 5, 14, and 23 are considered to avoid the influence of ground attenuation in lateral radiation. All microphone measurements were recorded using the "Slow" time weighting.
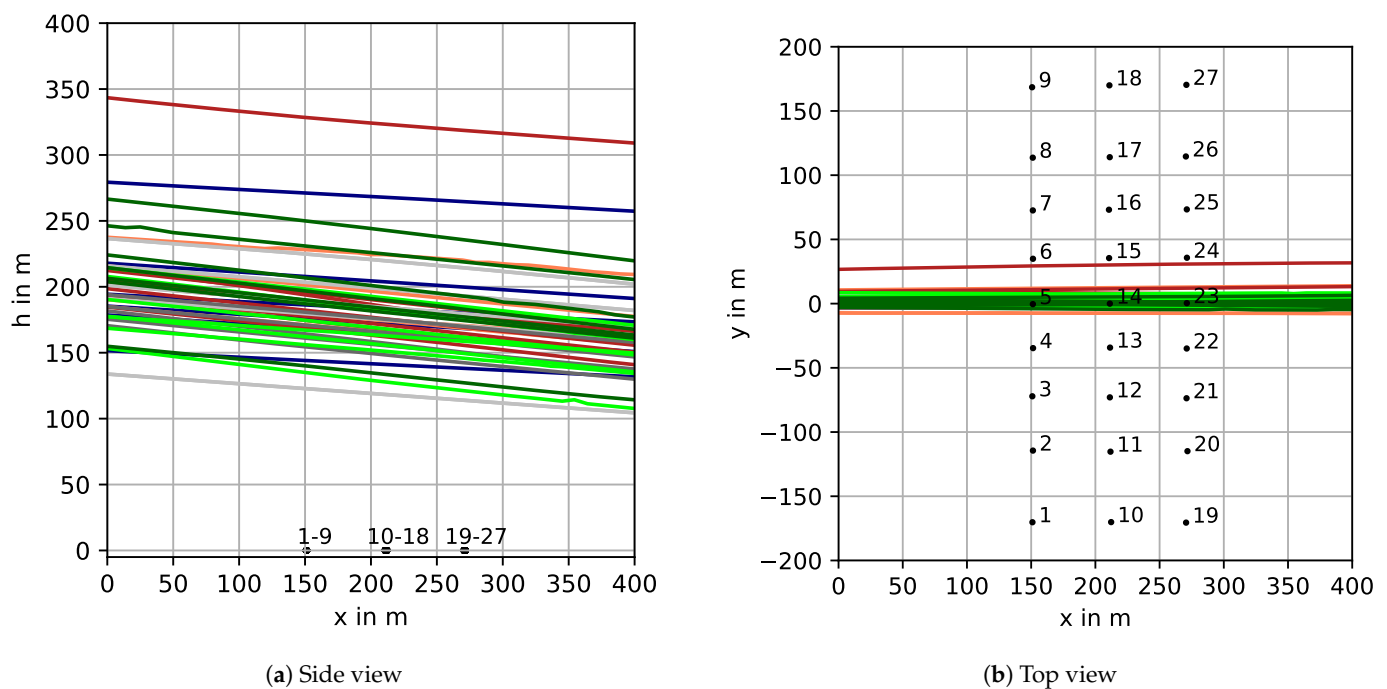

(**a**) Side view

(**b**) Top view

Figure 2. Flight trajectories and microphone positions of the flyover measurements. Color code according to Table 2.

As shown in Table 2, eight different configurations (A1, A2, B1, B2, C1, C2, D1, D2) were investigated during the flyover measurements. The parameters varied among the configurations, including the positions of the flaps, slats, and landing gear, as well as flight speed (true airspeed $TAS \approx 70\,\text{m/s}$ and $TAS \approx 90\,\text{m/s}$) resulting in Reynolds numbers ranging from $2.0 \cdot 10^7$ to $2.7 \cdot 10^7$. Compared to a previous assessment of the 2016 flight test, a more detailed distinction between the configurations is applied. In addition to the analysis presented in Bertsch et al. [13], different velocity regimes are investigated separately. Configurations tested at lower flight speeds are denoted by a "1" in the configuration label, whereas those conducted at higher flight speeds are marked by a "2". For each configuration, between five and nine flight repetitions were conducted. Within a given configuration, the true airspeed varied by no more than approximately $2\,\text{m/s}$ from the mean value presented in Table 2. As illustrated in Figure 2, the flyovers were performed at altitudes between $100\,\text{m}$ and $350\,\text{m}$. The objective of the measurement campaign from which the data were obtained was to examine the acoustic emission of airframe noise sources with minimal interference from other noise sources, which was achieved by operating the engines at idle thrust (see Bertsch et al. [13]). The tracking of landing approach trajectories has shown that, among the investigated configurations, A2 and D1 are the most relevant for aircraft of the A320 family during final approach [1]. Since the aircraft was flown at idle thrust during the measurements, the altitude decreased gradually during each flyover. The lateral deviation of the flight path from the centerline of the microphone array was less than $10\,\text{m}$ in all cases except for a single outlier. The trajectories in Figure 2 are colored according to the color code shown in Table 2.

Table 2. Aircraft configuration settings during the flyover measurement campaign.

Config.	Gear, %	Flap, °	Slat, °	TAS, m/s	Color Code	Number of Flights
A1	0	20	22	69	🔵	7
A2	0	20	22	92	🔵	6
B1	0	40	27	72	🟠	5
B2	0	40	27	89	🔴	9
C1	100	20	22	69	⚪	5
C2	100	20	22	92	⚫	5
D1	100	40	27	71	🟢	7
D2	100	40	27	90	🟢	7

4. Noise Simulation

4.1. Simulation Tools

The simulations of noise impact are carried out using PANAM [1]. PANAM calculates the frequency-resolved noise emission of individual noise sources on an aircraft as a function of emission angles based on parametric noise models. These noise sources can be classified into airframe and engine noise sources. The airframe noise sources are further divided into those originating from the clean airfoil, trailing-edge devices (flaps), leading-edge devices (slats), spoilers, and landing gear. The engine noise sources are categorized into jet noise and fan noise. Since jet noise does not make a significant contribution to the overall sound pressure level in any of the investigated cases, it will not be further discussed. Other acoustic sources are also not taken into account as they are negligible for the noise impact of the studied aircraft under the test flight conditions. Based on the noise emission, the sound propagation through the atmosphere is described using the sound propagation model ISO 9613 [28] and the influence of the ground effect is accounted for using the ground attenuation model described in ECAC Doc. 29 3rd Edition [29]. Table 3 provides an overview of the source models, sound propagation and ground attenuation models used in this study. A detailed description of the calculation methodology can be found in the literature [1,28–36]. For the present study, the measured trajectories and engine rotational speeds (N1) served as inputs for the simulations of the individual flyovers. At this point, it is important to emphasize that the flight operation is not simulated; instead, the measured parameters are directly provided to PANAM.

Table 3. Source and transmission models used for the noise simulation in PANAM. The model uncertainty values stem from literature and are explained in Section 4.2.

Noise Source	Model	Model Uncertainty (Standard Deviation σ)
Airframe noise models		
Slat	DLR [30,31]	1 dB [8]
Flap	DLR [31–33]	1 dB [8]
Landing gear	DLR [34]	1 dB [8]
Engine noise models		
Fan broadband & tonal	Modified Heidmann [35]	2 dB (isolated fan) [35] 3.6 dB (installed fan) [8,37]
Jet broadband	Modified Stone [36]	1.5 dB [8]
Transmission models		
Sound propagation model	ISO 9613 [28]	
Ground attenuation model	ECAC Doc. 29 3rd Edition [29]	

4.2. Uncertainty

In addition to the measured sound pressure levels, Figure 3 presents the calculated sound pressure level for the flyover in configuration A2, broken down into individual source contributions (airframe noise in dashed cyan, engine noise in green) as an illustrative example. To assess the prediction uncertainty of the simulation, the model uncertainties of the individual noise models are considered. The estimation of model uncertainties employed in this study is, where possible, based on specifications provided in the underlying documentation for each respective model or based on engineering judgement and experience. The model uncertainties are applied as derived within previous research activities. Comparing the uncertainties assumed in this study shows a good agreement to the documented choices of other researchers, e.g., June et al. [15] and Akatsuka and Ishii [5]. For each airframe noise model, an uncertainty with a standard deviation of 1 dB is assumed [8]. The model uncertainty of the installed fan noise is composed of the model uncertainty of the isolated fan and the uncertainty due to installation effects. These installation effects include acoustic lining in the inlet and exhaust duct, as well as shielding and reflection effects at the wing. For the isolated fan, Heidmann reports model uncertainties with a standard deviation of 2 dB [35]. The uncertainty in the installation effects is estimated with a standard deviation of 3 dB [8,37], resulting in a total model uncertainty of 3.6 dB for the installed fan noise. The uncertainty of the jet noise is lower than that of the fan noise, amounting to 1.5 dB [8]. Overall, the estimated uncertainty of the two engine noise components is consistent with the study by Envia et al. [38], who reported a total uncertainty of 4 dB for the overall engine noise of a similar aircraft. The grey shaded bands in Figure 3 indicate the error bands corresponding to one standard deviation of the individual noise sources.
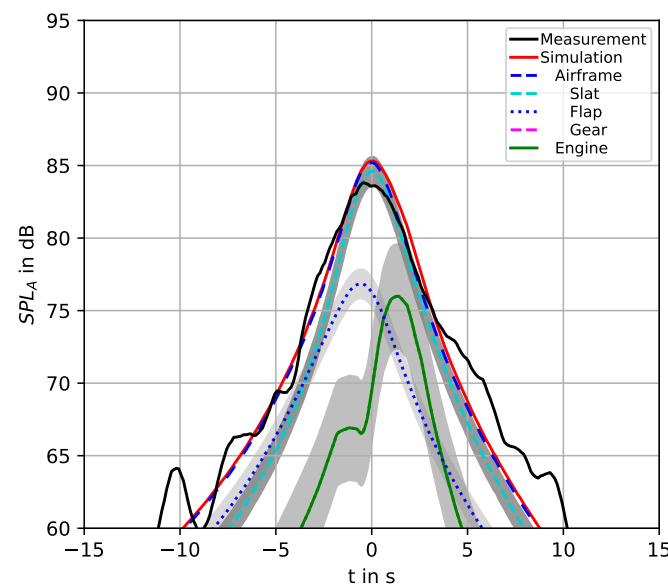

Figure 3. Level time history of an ATRA flyover in configuration A2 (Flight No. 44), recorded with microphone 5. Additionally, the simulated SPL_A of the individual noise sources and the total SPL_A are plotted. The uncertainties of the individual sources used in the simulation are represented by the grey bands (see also Table 3).

The model uncertainties of the individual noise sources are combined into an overall *SPL* uncertainty in two ways. First, the impact on the total *SPL* deviation is calculated by increasing (or decreasing) the *SPLs* of all individual sources by one standard deviation. Second, in a Monte Carlo simulation, the calculated *SPLs* of the individual noise sources are randomly perturbed according to their standard deviations, and these individual *SPLs*

are then energetically summed up to obtain the overall *SPL*. By repeating the simulation, the distribution of the calculated overall *SPL* is determined. Figure 4 shows the evolution of the mean value and standard deviation of the Monte Carlo simulation as the number of calculations increases for one flyover simulation. From this, it is evident that 1000 iterations are sufficient to achieve a converged solution. Whereas the calculation according to the first method represents a type of worst-case approximation, the calculation according to the second method yields a probability distribution of the simulation results.
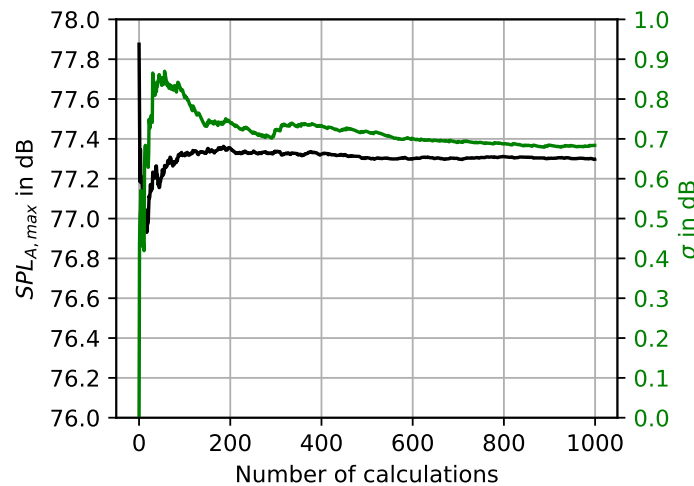

Figure 4. Evolution of the A-weighted maximum sound pressure level $SPL_{A,max}$ and its standard deviation σ with the number of Monte Carlo simulation runs for a flyover in configuration A1 (flight No. 28) at microphone 5.

5. Results and Discussion

This chapter discusses the measured and simulated A-weighted level time histories and the A-weighted maximum sound pressure levels of the ATRA flyovers. In Section 5.1, a comparison is made between the A-weighted maximum sound pressure levels of the studied configurations. The simulation results provide a detailed analysis of the aircraft's individual noise sources. Subsequently, the simulation results are compared with the measurements in Section 5.2, taking the model uncertainty into account.

5.1. Comparison of the Configurations

Since the flyovers were conducted at varying altitudes, the *SPLs* must be corrected to a uniform flight altitude to allow for a meaningful comparison between configurations. Figure 5 displays the maximum A-weighted sound pressure levels ($SPL_{A,max,corr}$) after correction to a reference altitude of 200 m above the microphone position recorded with the three centerline microphones as points. The correction for flight altitude is carried out based on the assumption of spherical sound propagation from a point source. Given the relatively short distances between the aircraft and the microphones, atmospheric effects are neglected in this correction. In addition to the sound pressure level, a correction of the flight altitude also affects the duration of the acoustic signal. For integral noise metrics such as the sound exposure level, altitude correction therefore results in slightly smaller deviations compared to the maximum levels. In the following, only corrections to the maximum sound pressure level are considered. Figure 5 also displays the 95% confidence intervals of the maximum A-weighted sound pressure levels as error bars. Numeric values are given in Table 4. The measurements within each configuration demonstrate high repeatability, with confidence intervals narrower than 1 dB. It should be noted that all flyovers were conducted on the same day. Repeated measurements on different days would likely result

in greater variation due to changes in atmospheric conditions. Moreover, the measurements from the three centerline microphones are not completely independent. If the same number of data points were obtained using only one microphone over three times as many flyovers, a higher variability in the values would also be expected.
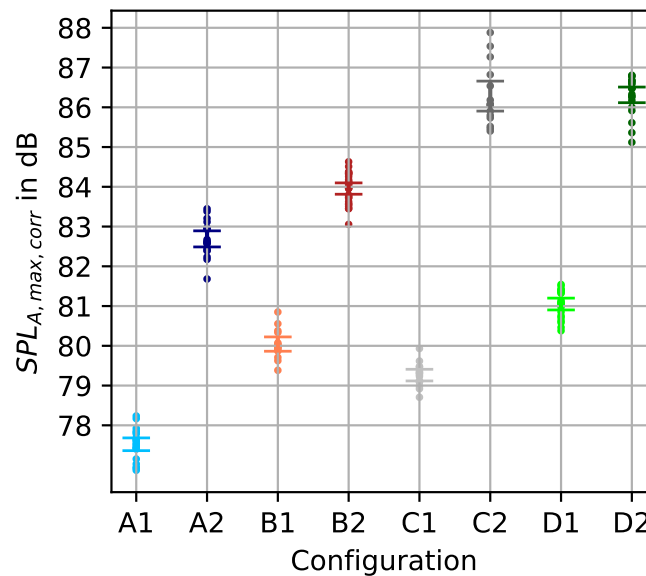

Figure 5. Maximum sound pressure level normalized to a flight altitude of 200 m ($SPL_{A,max,corr}$), recorded with the centerline microphones 5, 14, and 23 for ATRA flyovers in different configurations at idle thrust. The individual measurements are represented as points, the error bars represent the 95% confidence interval. The aircraft settings for the different configurations are shown in Table 2.

Table 4. Arithmetic mean and 95% confidence interval (CI) of the maximum sound pressure level normalized to a flight altitude of 200 m ($SPL_{A,max,corr}$) of the aircraft ATRA at idle thrust.

Config.	Measurement Mean (±Half-Width of 95% CI)	Simulation Mean (±Half-Width of 95% CI)	Difference
A1	77.5 (±0.16)	78.9 (±1.42)	+1.4
A2	82.7 (±0.20)	84.6 (±1.72)	+1.9
B1	80.0 (±0.18)	80.0 (±1.43)	0
B2	84.0 (±0.14)	84.5 (±1.78)	+0.5
C1	79.3 (±0.15)	80.0 (±1.20)	+0.7
C2	86.3 (±0.38)	87.1 (±1.44)	+0.8
D1	81.1 (±0.15)	81.3 (±1.36)	+0.2
D2	86.3 (±0.20)	87.0 (±1.38)	+0.7

For each of the eight configurations, Figure 6 presents a measured and simulated level time history for a single flyover. Time is set such a way that $t = 0$ s corresponds to the time for which the sound pressure levels of the simulations have their maximum. Since the measurements were conducted at different flight altitudes, the SPL values between individual flyovers are not directly comparable. At lower altitudes, the aircraft passes the microphone more quickly, resulting in sharper, higher peaks. The simulated sound-pressure-level time histories show the contributions of different sources over time. Since the overall noise of the flyovers results from an energetic summation of the levels of the individual noise sources, it is usually dominated by the loudest sources. As illustrated in Figure 6, the ranking of the sources depends on the configuration of the aircraft.
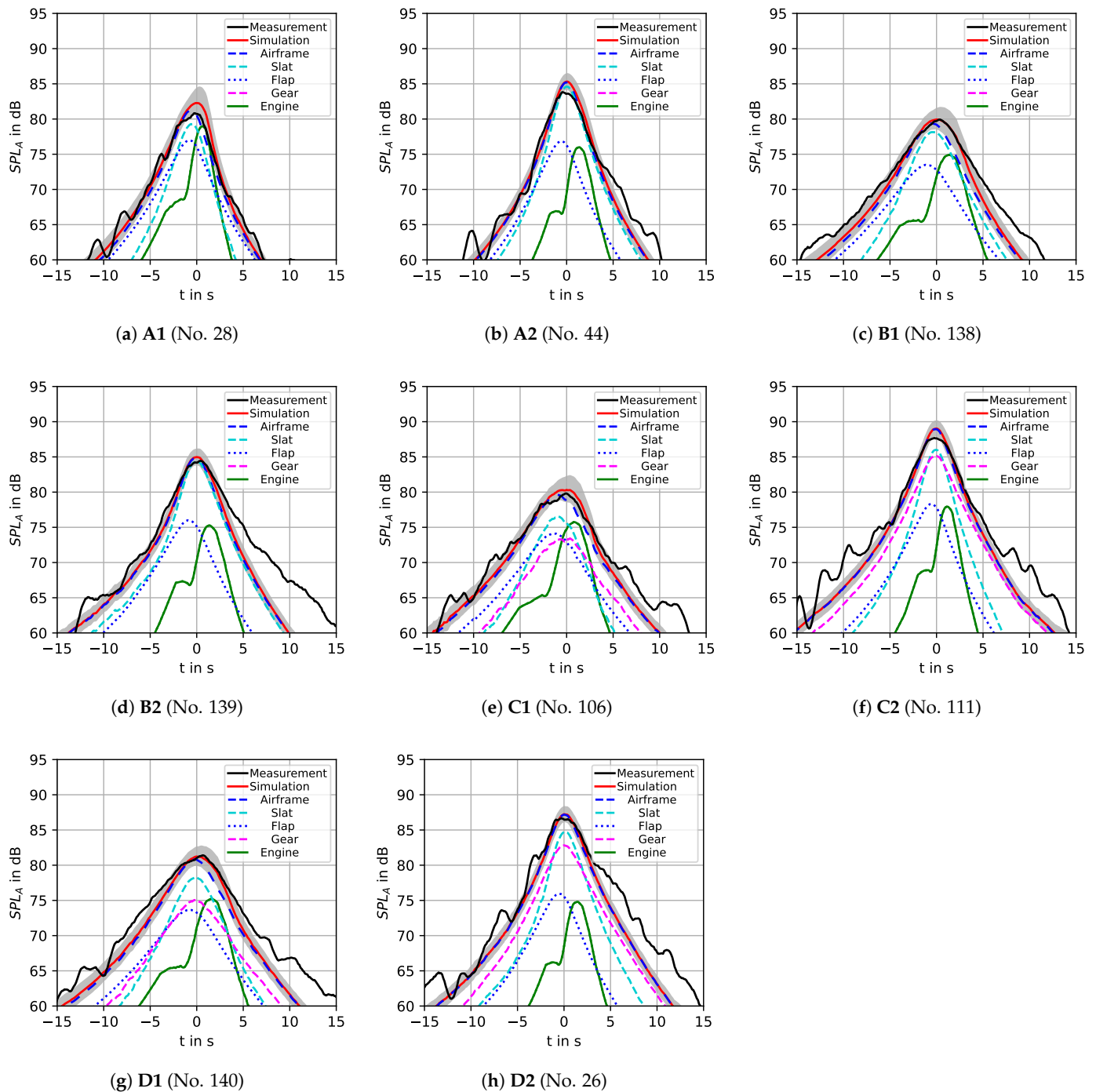
Figure 6. Level time history of ATRA flyovers for the different configurations at idle thrust, recorded with microphone 5. The grey bands represent the simulations obtained by adding or subtracting one standard deviation of the model uncertainty to all individual noise sources.

At time intervals greater than approximately 5 s from the point of maximum level, the measured level time history exhibits fluctuations for some flights. These fluctuations are attributed to unsteady atmospheric conditions. However, since the levels lie at least 15 dB below the maximum sound pressure level, their contribution to the total acoustic energy is negligible.

Since the engines are operating in idle, the jet noise is negligible and lies below the level range shown in Figure 6. The engine noise, shown in green, is solely emitted by the fan. It significantly contributes to the measured total noise only at lower flight speeds

(A1, B1, C1, D1). In contrast, at higher flight speeds (A2, B2, C2, D2) at least one airframe noise source dominates over the fan noise. The reason for this is that the noise generation of aerodynamic noise sources strongly depends on the flight speed (theoretically sound power $P \sim v^6$ [39]), whereas the influence of flight speed on the fan noise is not that high. Moreover, it is noteworthy that the fan noise reaches its maximum in time, always after the airframe noise maximum. Figures A1 and A2 show the time level time history for the centerline microphones 14 and 23. Qualitatively, the results are consistent with those obtained at microphone 5.

5.1.1. Effect of Flight Speed

As depicted in Figure 5, the flyovers at higher speeds (A2, B2, C2, D2) in general exhibit higher sound pressure levels than the slower flyover (A1, B1, C1, D1). The reason for this is that the acoustic power of the noise sources increases proportionally to a power of the flight velocity. Specifically, the emitted acoustic power scales with v^5 for slat and flap noise [1], and with v^6 for landing gear noise [34]. For configurations A and B, the fan and slat are dominant at lower speeds, while at higher speeds, only the slat is dominant. The increase in speed results in an increase in 5.2 dB for configuration A and 4.0 dB for configuration B. This corresponds to speed-dependence exponents of 4.8 and 3.7, respectively. For configurations C and D, the fan and slat dominate at lower speeds, whereas the slat and gear dominate at higher speeds. For these configurations, the higher speeds result in an increase of 7.0 dB and 5.2 dB, corresponding to speed-dependence exponents of 6.4 and 4.8, respectively.

5.1.2. Effect of Flap/Slat Deployment

First, the focus is on the comparison of the configurations flown at 70 m/s (A1, B1). Figure 5 reveals that increasing the flap and slat deflection angle from 20°/22°(A1) to 40°/27°(B1) leads to an increase in noise impact by 2.5 dB. As shown in Figure 6, the simulated noise source breakdown attributes this increase to a relative rise in slat noise.

At higher velocities (A2, B2), increasing the flap and slat deflection angle from 20°/22°to 40°/27°the maximum SPL also increases; however, the rise of 1.3 dB is lower compared to lower flight speeds.

When the landing gear is deployed, the deployment of the flaps results in smaller increases in the maximum SPL. At low speeds (C1, D1) this increase is 1.8 dB, while at higher speeds (C2, D2) the maximum SPL remains constant. This arises from the fact that the gear noise is of the same order of magnitude as the slat noise. Hence, the additional slat noise generated by full flap deployment has a less pronounced effect on the overall maximum SPL.

5.1.3. Effect of Gear Deployment

Relative to the reference configuration (A1), deploying the landing gear (C1) results in an average SPL increase of 1.8 dB (see Figure 5). Figure 6 shows that while the ranking of slat, flap, and engine noise remains unchanged, the additional landing gear noise source accounts for the increase.

Comparing flap/slat deployment with landing gear deployment at low speeds (A1, B1, C1) shows that the effect of flap deployment on the maximum SPL is 2.5 dB, which is stronger than the effect of landing gear deployment, leading to a 1.8 dB increase. This trend reverses at higher speeds of 90 m/s (A2, B2, C2): Under these conditions, flap deployment results in an increase of only 1.3 dB, whereas landing gear deployment causes a rise of 3.6 dB. The stronger increase in landing gear noise compared to the slat noise with increasing speed is due to the fact that the sound power of the gear noise scales proportionally with v^6 [34], whereas for the slat noise it scales with v^5 [40].

5.2. Comparison of Measurement and Simulation

A meaningful comparison between the measurements and the calculations is only possible when the associated uncertainties are taken into account. Figure 6 presents, in addition to the measurement and simulation results, the range (shown in gray) that the simulation would exhibit if the sound pressure levels of all individual noise sources were increased or decreased by their respective standard deviation (worst-case approximation). For comparison, Figure 7 displays the interval covering 95% of the Monte Carlo simulation results, based on the uncertainties of the individual noise sources (see also in Section 4.2). The comparison of the two types of uncertainty estimations in Figures 6 and 7 shows that the interval between the worst-case approximation and the interval containing 95% of the Monte Carlo simulations are similar.
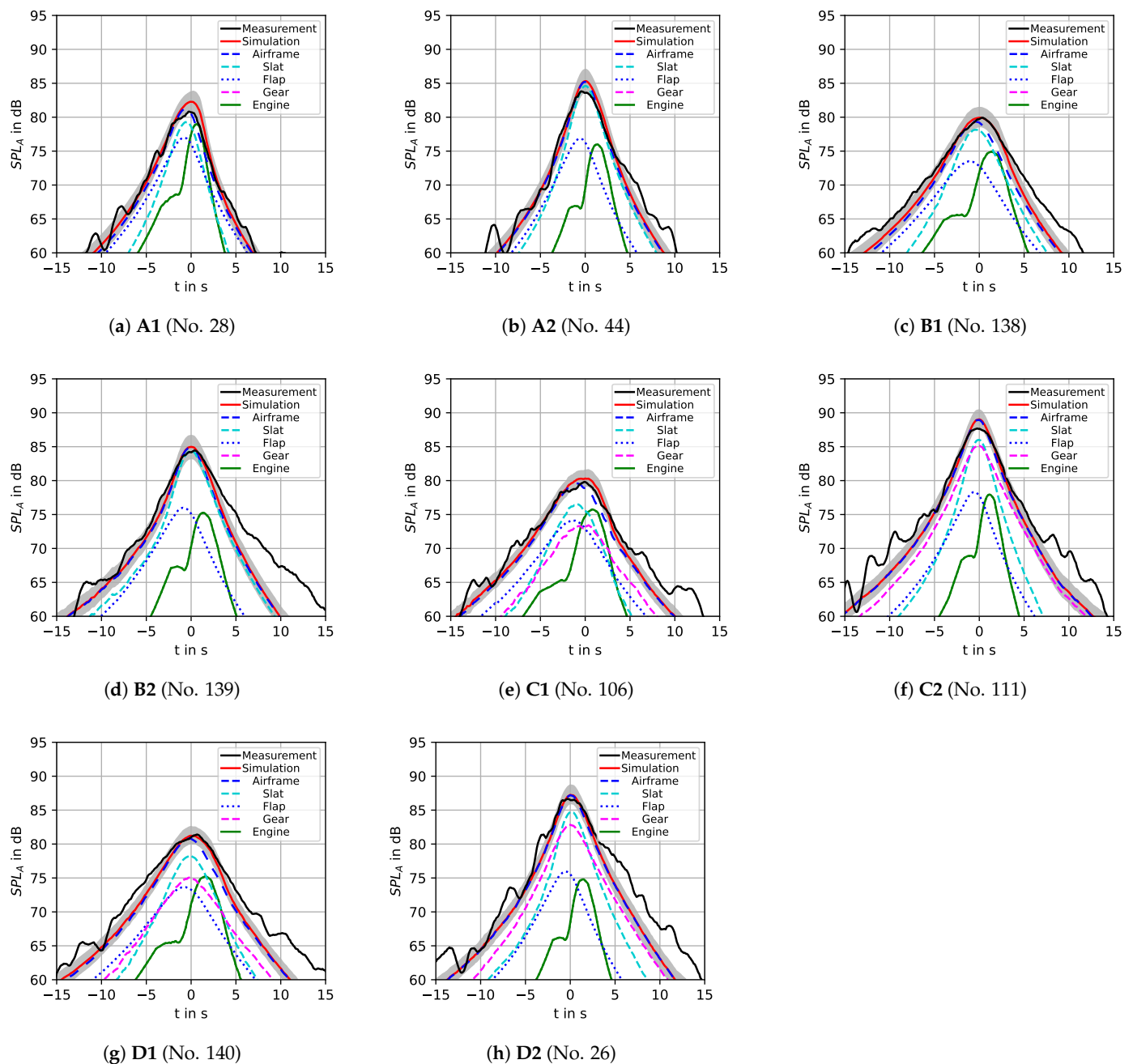

Figure 7. Level time history of ATRA flyovers for the different configurations at idle thrust, recorded with microphone 5. The grey bands contain 95% of the Monte Carlo simulations.

For all configurations shown in Figures 6 and 7, the time of the maximum sound pressure level and the level rise and fall close to the peak agree well between simulation and measurement. The fluctuations observed in the measurements at lower levels before and after the aircraft passes directly over the microphone suggest an influence from atmospheric disturbances and from more complex ground reflections at shallow incidence angles. A further reason for the larger fluctuations in this region is the increased influence of background noise at lower $SPLs$. The simulation does not account for either atmospheric disturbances or background noise.

As illustrated in Figures 6 and 7, the simulations yield a narrow uncertainty interval for the expected total sound pressure level. This interval widens when fan noise becomes dominant, since the model uncertainty of 3.6 dB standard deviation, this uncertainty is significantly greater than the model uncertainties of the aerodynamic noise sources.

Figure 8 presents the measurements from the centerline microphones of the maximum normalized SPL along with the corresponding 95% confidence intervals indicated by grey bands (see also Figure 5). In addition, the intervals covering 95% of the Monte Carlo simulation for the individual flyovers are shown as error bars, while those considering all flyovers are represented by colored bands. Table 4 lists the arithmetic mean of the maximum SPL from the experiment and the simulation.

The comparison between measurements and simulations for the configurations B, C, and D in Table 4 shows that the simulations $SPL_{A,max,corr}$ overestimate the noise impact by up to 0.8 dB. For these cases Figure 8c–h shows that the interval containing 95% of the Monte Carlo simulations overlaps with the 95% confidence interval of the measurements. By contrast, for the configurations A1 and A2 the simulation overestimates the noise by an average of 1.4 dB and 1.9 dB, respectively. Figure 8a,b indicate that the error bars of the simulations no longer overlap with the measurement 95% confidence intervals. This suggests that a systematic error occurs in the calculation of the aircraft noise. Figure 6a,b show that, for these configurations (particularly A2), the slat noise is the dominant contributor to the overall SPL. This shows that either the model uncertainty for slat noise was underestimated, or that the slat noise model needs to be adjusted to achieve better agreement between experiment and simulation. Improvements could, for example, be achieved by employing a high-fidelity simulation of slat noise instead of the empirical slat model currently used in PANAM.
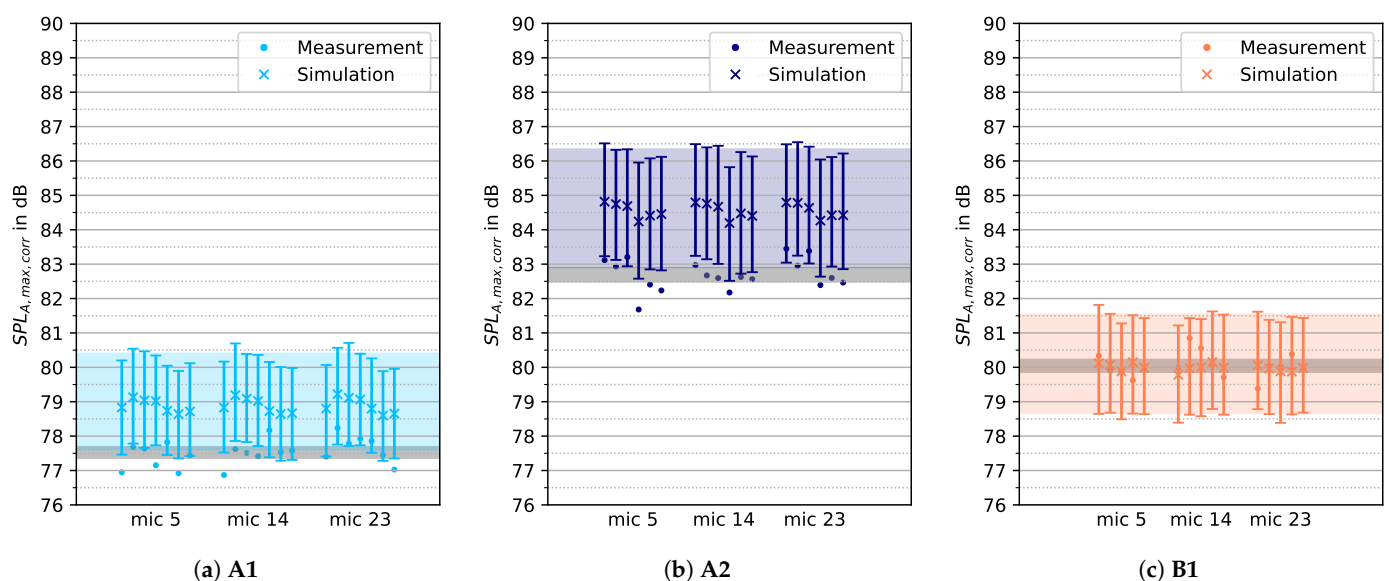

(a) A1   (b) A2   (c) B1

Figure 8. *Cont.*

(d) B2

(e) C1
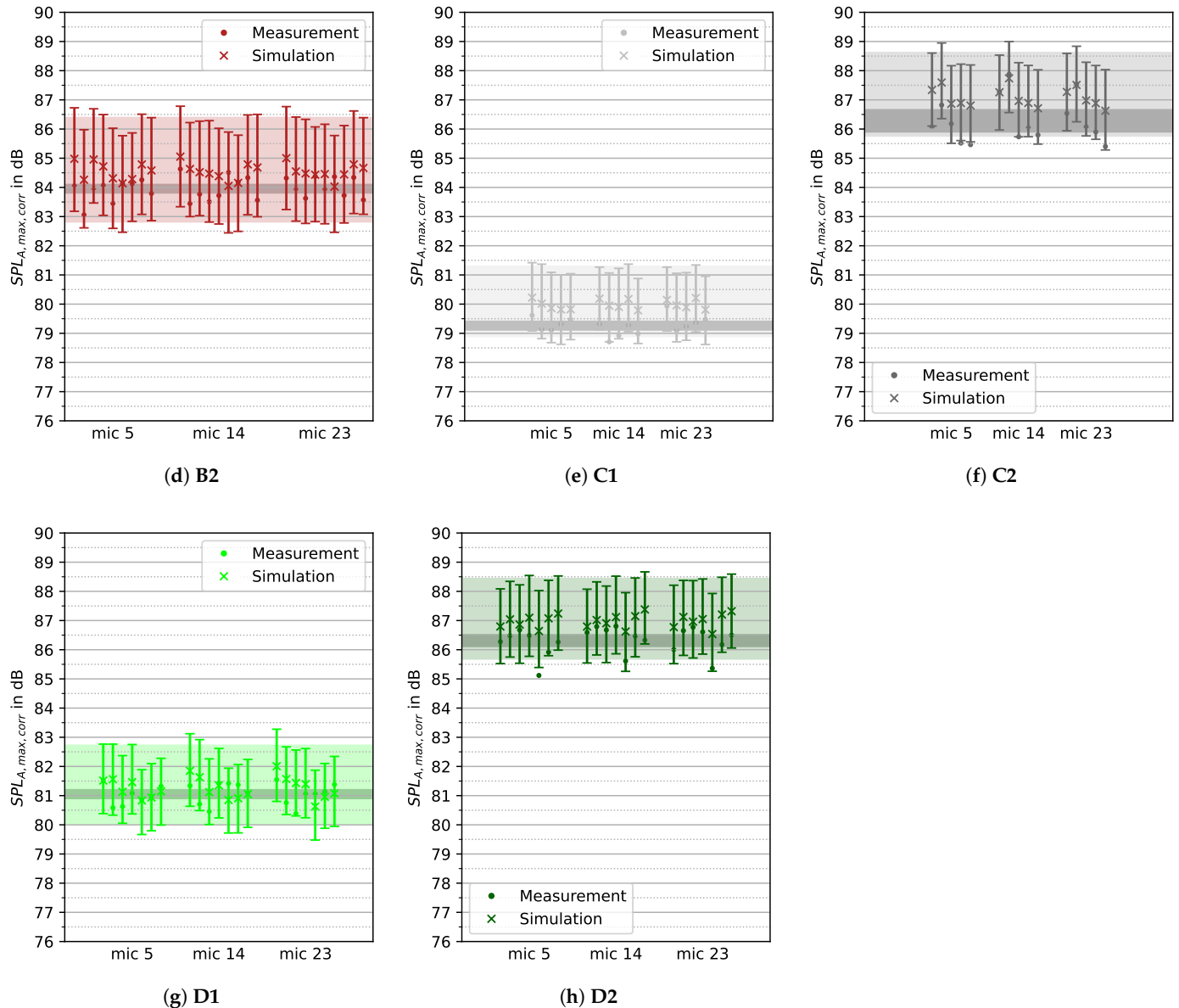
(f) C2

(g) D1

(h) D2

Figure 8. Maximum sound pressure level of ATRA flyover measurements at idle thrust and simulations for the centerline microphones 5, 14, and 23, normalized to a flight altitude of 200 m ($SPL_{A,max,corr}$). The simulations are shown with error bars containing 95% of the Monte Carlo simulations. The grey band represents the 95% confidence interval of the measurements.

6. Conclusions

In this study, flyover measurements obtained using the DLR's experimental aircraft ATRA were compared with simulations performed using the parametric noise assessment code PANAM. The comparison considered eight different slat, flap, and landing gear approach configurations at idle thrust for two different velocities. The focus was on comparing measurement and simulation results, accounting for the model uncertainties of the applied noise source models. For this purpose, Monte Carlo simulations were performed to quantify the uncertainty range of the simulation results.

To the best of the authors' knowledge, this is the first study to combine the comparison of flyover measurements with simulations and the assessment of uncertainties. Previous studies have focused either on comparing measurements and simulations [13,41,42] or on evaluating simulation uncertainties [5–7,10,14–17].

The results indicate that the PANAM simulations of the maximum A-weighted sound pressure level encompass the 95% confidence intervals of the measurement for six out of the eight configurations. The results demonstrate that the PANAM noise simulation accurately reproduces the actual noise exposure during the ATRA approach. Only for the two configurations with flaps deployed at 20° and slats at 22° (configuration A1 and A2), the PANAM predictions of the maximum sound pressure level overestimate the measured data by an average of up to 1.9 dB. Since slat noise is the dominant source in these two configurations, either the model uncertainty for slat noise at a slat deflection angle of 22° is underestimated, or the slat noise model systematically overestimates the emission levels for the investigated aircraft.

A comparison of flyover measurements with PANAM simulations for the ATRA was already conducted by Bertsch et al. [13]. However, a detailed uncertainty analysis was not within the scope of that paper. In their study, the simulations showed good agreement with the measurement results, although the simulations tended to slightly overestimate the observed values. For the ATRA, the deviations were below 2 dB, which is consistent with the mean deviations between simulation and measurement reported in the present study.

To further improve the accuracy of the PANAM noise simulations, future work will focus on calibrating the current slat noise model, which is based on parametric wind-tunnel data, using acoustic high-fidelity simulations for selected flight conditions. However, due to the high computational cost of such high-fidelity simulations, their direct use in total aircraft assessment codes such as PANAM remains impractical; approximative approaches, i.e., mixed-fidelity approaches, become essential.

Author Contributions: Conceptualization, F.L., L.B., and R.S.; methodology, F.L., L.B., and R.S.; software, L.B.; validation, L.B. and F.L.; investigation, F.L.; writing—original draft preparation, F.L.; writing—review and editing, R.S. and L.B.; visualization, F.L. All authors have read and agreed to the published version of the manuscript.

Conflicts of Interest: The authors declare no conflicts of interest.

Abbreviations

The following abbreviations are used in this paper:

ANOPP	Aircraft Noise Prediction Program
ATRA	Advanced Technology Research Aircraft
CI	Confidence interval
DLR	German Aerospace Center
JAXA	Japan Aerospace Exploration Agency
NASA	National Aeronautics and Space Administration
P	Sound power, W
PANAM	Parametric Aircraft Noise Analysis Module
PrADO	Preliminary Aircraft Design and Optimization
SPL	Sound pressure level, dB
SPL_A	A-weighted sound pressure level, dB
$SPL_{A,max,corr}$	Maximum A-weighted sound pressure level, corrected for an altitude of 200 m, dB
TAS	True airspeed, m/s
σ	Standard deviation

Appendix A

(**a**) **A1** (No. 28)

(**b**) **A2** (No. 44)

(**c**) **B1** (No. 138)

(**d**) **B2** (No. 139)

(**e**) **C1** (No. 106)

(**f**) **C2** (No. 111)

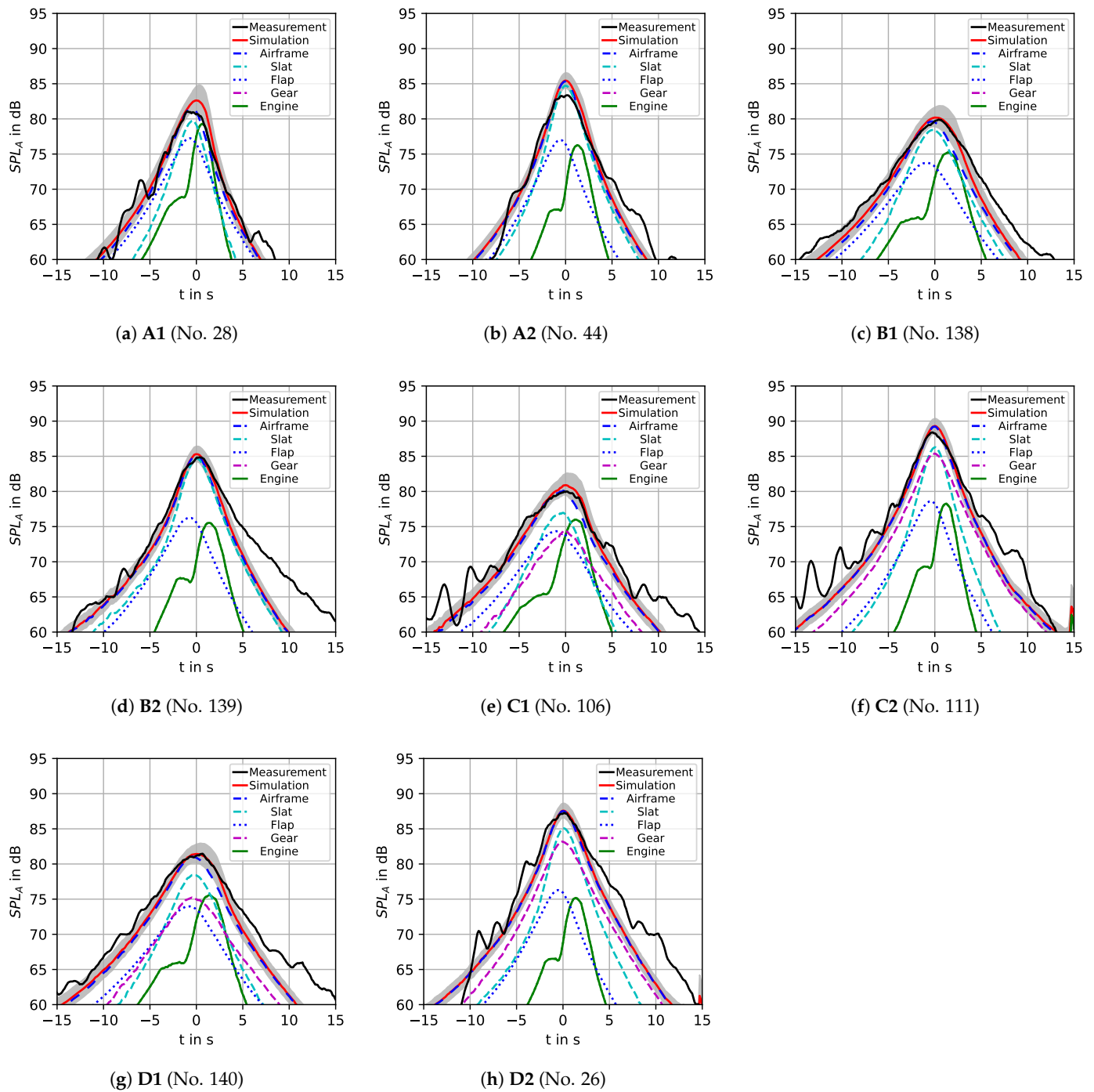(**g**) **D1** (No. 140)

(**h**) **D2** (No. 26)

Figure A1. Level time history of ATRA flyovers for the different configurations at idle thrust, recorded with microphone 14. The grey bands represent the simulations obtained by adding or subtracting one standard deviation of the model uncertainty to all individual noise sources.

Figure A2. Level time history of ATRA flyovers for the different configurations at idle thrust, recorded with microphone 23. The grey bands represent the simulations obtained by adding or subtracting one standard deviation of the model uncertainty to all individual noise sources.
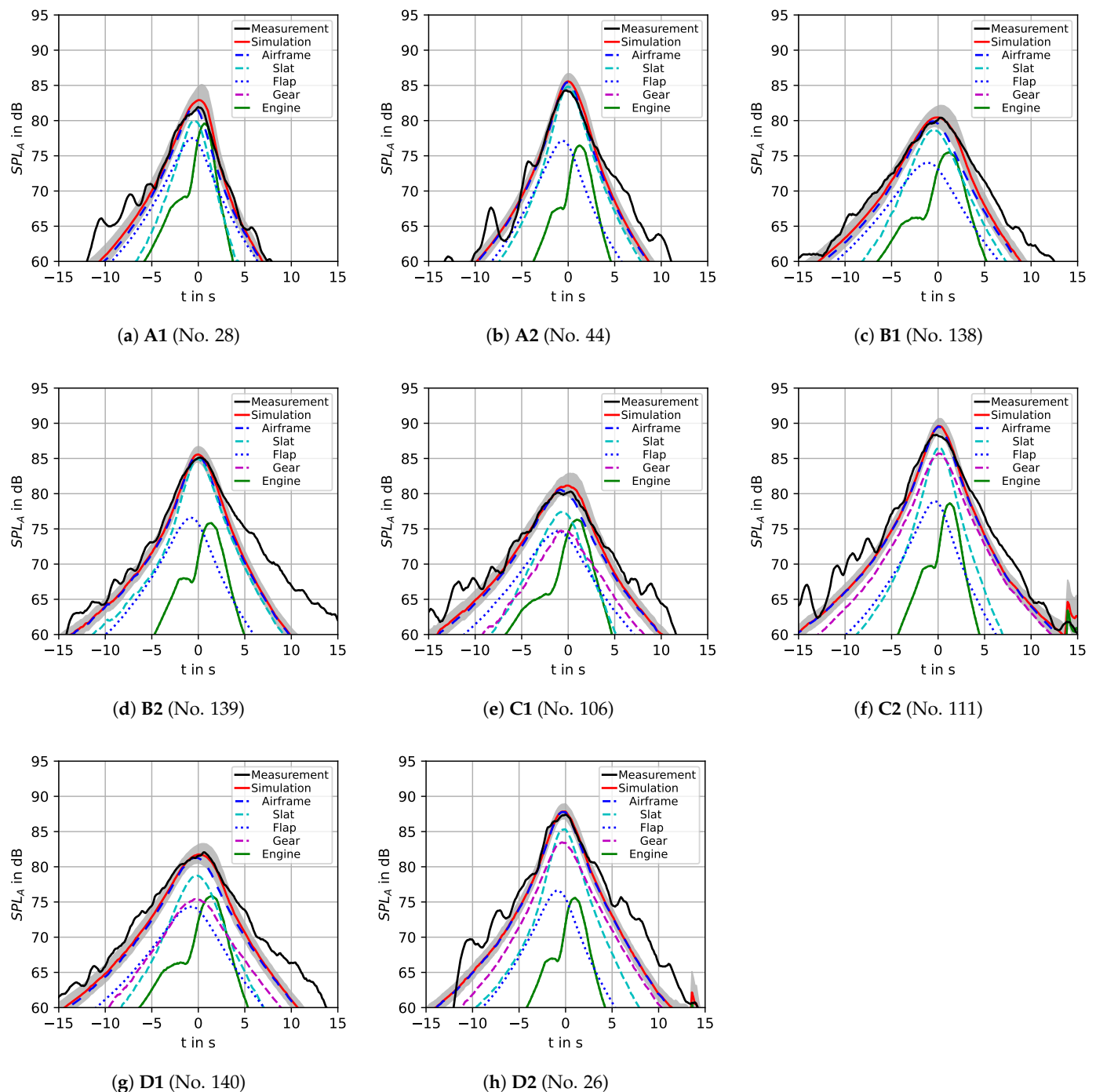
References

1.　Bertsch, L. *Noise Prediction Within Conceptual Aircraft Design*; Technical Report; DLR, Institute of Aerodynamics and Flow Technology: Braunschweig, Germany, 2013. [CrossRef]
2.　Lopes, L.; Burley, C. Design of the Next Generation Aircraft Noise Prediction Program: ANOPP2. In Proceedings of the 17th AIAA/CEAS Aeroacoustics Conference, Portland, OR, USA, 5–8 June 2011. [CrossRef]
3.　Jäger, D.; Zellmann, C.; Schlatter, F.; Wunderli, J. Validation of the sonAIR aircraft noise simulation model. *Noise Mapp.* **2021**, *8*, 95–107. [CrossRef]
4.　Wunderli, J.; Meister, J.; Jäger, D.; Schalcher, S.; Zellmann, C.; Schäffer, B. Aircraft noise in situations with grazing sound incidence—Comparing different modeling approaches. *J. Acoust. Soc. Am.* **2022**, *151*, 3140–3151. [CrossRef] [PubMed]

5. Akatsuka, J.; Ishii, T. System noise assessment and uncertainty analysis of a conceptual supersonic aircraft. *Aerospace* **2022**, *9*, 212. [CrossRef]

6. Akatsuka, J. Sensitivity Analysis of Landing and Takeoff Noise for Conceptual Low-Boom Supersonic Aircraft Using Variable noise Reduction System. In Proceedings of the Internoise 2024, Nantes, France, 25–29 August 2024. [CrossRef]

7. Akatsuka, J.; Ueno, A.; Makino, Y. System Noise Assessment and Prediction Methodology Uncertainty Analysis for JAXA's Supersonic Conceptual Aircraft with Variable Noise Reduction System. In Proceedings of the AIAA SciTech 2025 Forum, Orlando, FL, USA, 6–10 January 2025. [CrossRef]

8. Bertsch, L.; Schäffer, B.; Guérin, S. Uncertainty analysis for parametric aircraft system noise prediction. *J. Aircr.* **2019**, *56*, 529–544. [CrossRef]

9. Römer, U.; Bertsch, L.; Mulani, S.; Schäffer, B. Uncertainty quantification for aircraft noise emission simulation: Methods and limitations. *AIAA J.* **2022**, *60*, 3020–3034. [CrossRef]

10. Bertsch, L.; Lößle, F.; Nöding, M.; Schäffer, B.; Mulani, S. Uncertainty quantification of single event noise predictions for conceptual supersonic transport aircraft. *J. Aircr.* **2025**. [CrossRef]

11. Vieira, A.; von den Hoff, B.; Snellen, M.; Simons, D. Comparison of semi-empirical noise models with flyover measurements of operating aircraft. *J. Aircr.* **2022**, *59*, 1574–1587. [CrossRef]

12. Thoma, E.; Grönstedt, T.; Sola, E.; Zhao, X. Assessment of an open-source aircraft noise prediction model using approach phase measurements. *J. Aircr.* **2024**, *61*, 745–760. [CrossRef]

13. Bertsch, L.; Pott-Polenske, M.; Wienke, F.; Kurz, J.; Delfs, J. Retrofit measurement for aircraft noise reduction: Simulation benchmark and impact assessment. *J. Aircr.* **2024**, *62*, 191–206. [CrossRef]

14. Burley, C.; Thomas, R.; Guo, Y. Quantification of Acoustic Scattering Prediction Uncertainty for Aircraft System Noise Assessment. In Proceedings of the 22nd AIAA/CEAS Aeroacoustics Conference, Lyon, France, 30 May–1 June 2016. [CrossRef]

15. June, J.; Thomas, R.; Guo, Y. System noise prediction uncertainty quantification for a hybrid wing–body transport concept. *AIAA J.* **2020**, *58*, 1157–1170. [CrossRef]

16. Bridges, J.; Stephens, D.; Berton, J. Quantifying Uncertainty of Landing and Takeoff Noise for Commercial Supersonic Aircraft. In Proceedings of the 28th AIAA/CEAS Aeroacoustics Conference, Southhampton, UK, 14–17 June 2022. [CrossRef]

17. Bridges, J. Results of the NASA Prediction Uncertainty Reduction Tech Challenge. In Proceedings of the AIAA SciTech 2025 Forum, Orlando, FL, USA, 6–10 January 2025. [CrossRef]

18. Siller, H.; Hage, W.; Schumacher, T. Source Localisation on Aircraft in Flight—New Measurements with the DLR Research Aircraft Airbus 320 ATRA. In Proceedings of the 7th Berlin Beamforming Conference, Berlin, Germany, 5–6 March 2018.

19. Siller, H.; Schumacher, T.; Hage, W. Low Noise ATRA-Phased Array Measurements of Jet Noise in Flight. In Proceedings of the AIAA Aviation 2021 Forum, Virtual Event, 2–6 August 2021. [CrossRef]

20. Pott-Pollenske, M. Low Noise ATRA—An Aircraft Noise Reduction Study Based on Retro-Fit Technologies. In Proceedings of the AIAA Aviation 2021 Forum, Virtual Event, 2–6 August 2021. [CrossRef]

21. Garg, N.; Surendran, P.; Dhanya, M.; Chandran, A.; Asif, M.; Singh, M. Measurement uncertainty in microphone free-field comparison calibrations *MAPAN J.* **2019**, *34*, 357–369. [CrossRef]

22. Heinze, W. *Ein Beitrag zur Quantitativen Analyse der Technischen und Wirtschaftlichen Auslegungsgrenzen Verschiedener Flugzeugkonzepte für den Transport Großer Nutzlasten*; Institute of Aircraft Design and Lightweight Structures: Braunschweig, Germany, 1994.

23. Heinze, W.; Oesterheld, C.M.; Horst, P. Multidisziplinäres Flugzeugentwurfsverfahren PrADO—Programmentwurf und Anwendung im Rahmen von Flugzeugkonzeptstudien. In Proceedings of the DLRK, Hamburg, Germany, 17–20 September 2001.

24. Bertsch, L.; Heinze, W.; Lummer, M. Application of an Aircraft Design-to-Noise Simulation Process. In Proceedings of the 14th AIAA Aviation Technology, Integration, and Operations Conference, Atlanta, GA, USA, 16–20 June 2014.

25. Bertsch, L.; Wienke, F.; Blinstrub, J.; Iwanizki, M.; Balack, P.; Häßy, J. System noise of tube-and-wing and blended-wing–body concept aircraft. *J. Aircr.* **2025**, *62*, 915–928. [CrossRef]

26. Becker, R.; Wolters, F.; Nauroz, M.; Otten, T. Development of a Gas Turbine Performance Code and Its Application to Preliminary Engine Design. In Proceedings of the Deutscher Luft- und Raumfahrtkongress 2011 (DLRK), Bremen, Germany, 27–29 September 2011.

27. German Aerospace Center (DLR). Airbus A320-232 D-ATRA. Available online: https://www.dlr.de/de/forschung-und-transfer/forschungsinfrastruktur/dlr-forschungsflotte/airbus-a320-232-d-atra (accessed on 11 August 2025).

28. *ISO 9613-1:1993*; Acoustics—Attenuation of Sound During Propagation Outdoors. Part 1: Calculation of the Absorption of Sound by the Atmosphere. International Organization for Standardization, Geneva, Switzerland, 1993.

29. European Civil Aviation Conference. *Methodology for Computing Noise Contours Around Civil Airports. Volume 2: Technical Guide*, 3rd ed.; ECAC Doc. 29; European Civil Aviation Conference: Paris, France, 2005.

30. Dobrzynski, W.; Pott-Pollenske, M. Slat Noise Source Studies for Farfield Noise Prediction. In Proceedings of the 7th AIAA/CEAS Aeroacoustics Conference and Exhibit, Maastricht, The Netherlands, 28–30 May 2001. [CrossRef]

31. Pott-Pollenske, M.; Dobrzynski, W.; Buchholz, H.; Gehlhar, B.; Walle, F. Validation of a Semiempirical Airframe Noise Prediction Method Through Dedicated A319 Flyover Noise Measurements. In Proceedings of the 8th AIAA/CEAS Aeroacoustics Conference and Exhibit, Breckenridge, CO, USA, 17–19 June 2002. [CrossRef]

32. Rossignol, K. Development of an Empirical Prediction Model for Flap Side-Edge Noise. In Proceedings of the 16th AIAA/CEAS Aeroacoustics Conference and Exhibit, Stockholm, Sweden, 7–9 June 2010. [CrossRef]

33. Rossignol, K. Empirical Prediction of Flap Tip Noise. In Proceedings of the 17th AIAA/CEAS Aeroacoustics Conference and Exhibit, Portland, OR, USA, 5–8 June 2011. [CrossRef]

34. Dobrzynski, W.; Chow, L.; Guion, P.; Shiells, D. A European Study on Landing Gear Airframe Noise Sources. In Proceedings of the 6th AIAA/CEAS Aeroacoustics Conference and Exhibit, Lahaina, HI, USA, 12–14 June 2000. [CrossRef]

35. Heidmann, M. *Interim Prediction Method for Fan and Compressor Source Noise*; Technical report, NASA Technical Memorandum X-71763; NASA: Washington, D.C., USA, 1979.

36. Stone, J.R.; Groesbeck, D.E.; Zola, C.L. Conventional profile coaxial jet noise prediction. *AIAA J.* **1983**, *21*, 336–342. [CrossRef]

37. Lummer, M. Maggi-Rubinowicz Diffraction Correction for Ray-Tracing Calculations of Engine Noise Shielding. In Proceedings of the 14th AIAA/CEAS Aeroacoustics Conference, Vancouver, BC, Canada, 5–7 May 2008. [CrossRef]

38. Envia, E.; Tweedt, D.; Woodward, R.; Elliott, D.; Fite, E.; Hughes, C.; Podboy, G.; Sutliff, D. An Assessment of Current Fan Noise Prediction Capability. In Proceedings of the 14th AIAA/CEAS Aeroacoustics Conference, Vancouver, BC, Canada, 5–7 May 2008. [CrossRef]

39. Goldstein, M. *Aeroacoustics*; Technical Report, NASA Special Publication SP-346; NASA: Washington, DC, USA, 1974.

40. Pott-Pollenske, M.; Dobrzynski, W.; Buchholz, H.; Guérin, S.; Saueressig, G.; Finke, U. Airframe Noise Characteristics from Flyover Measurements and Prediction. In Proceedings of the 12th AIAA/CEAS Aeroacoustics Conference, Cambridge, MA, USA, 8–10 May 2006. [CrossRef]

41. Thomas, R.; Guo, Y.; Clark, I.; June, J. Propulsion Airframe Aeroacoustics and Aircraft System Noise Flight Research Test: NASA Overview. In Proceedings of the 28th AIAA/CEAS Aeroacoustics Conference, Southhampton, UK, 14–17 June 2022. [CrossRef]

42. Guo, Y.; Thomas, R. Assessment of Next Generation Airframe System Noise Prediction Methods with PAA and ASN Flight Test Data. In Proceedings of the 28th AIAA/CEAS Aeroacoustics Conference, Southhampton, UK, 14–17 June 2022. [CrossRef]